Phonon-Mediated Electron Transport through CaO Thin Films

Yi Cui,[1] Sergio Tosoni,[2] Wolf-Dieter Schneider,[1,3] Gianfranco Pacchioni,[2] Niklas Nilius,[1,4,*] and Hans-Joachim Freund[1]
[1]*Fritz-Haber-Institut der Max-Planck-Gesellschaft, Faradayweg 4-6, 14195 Berlin, Germany*
[2]*Dipartimento di Scienza dei Materiali, Università di Milano-Bicocca, via Cozzi 53, 20125 Milano, Italy*
[3]*Ecole Polytechnique Fédérale de Lausanne, Institute of Physics, CH-1015 Lausanne, Switzerland*
[4]*Carl von Ossietzky Universität Oldenburg, Institut für Physik, D-26111 Oldenburg, Germany*
(Received 28 May 2014; published 7 January 2015)

Scanning tunneling microscopy has developed into a powerful tool for the characterization of conductive surfaces, for which the overlap of tip and sample wave functions determines the image contrast. On insulating layers, as the CaO thin film grown on Mo(001) investigated here, direct overlap between initial and final states is not enabled anymore and electrons are transported via hopping through the conduction-band states of the oxide. Carrier transport is accompanied by strong phonon excitations in this case, imprinting an oscillatory signature on the differential conductance spectra of the system. The phonons show a characteristic spatial dependence and become softer around lattice irregularities in the oxide film, such as dislocation lines.

DOI: 10.1103/PhysRevLett.114.016804 PACS numbers: 73.40.Ns, 63.20.kd, 68.37.Ef, 73.61.Ng

Phonons, as fundamental excitations of the crystal lattice, are inherent to many solid-state phenomena occurring on time scales longer than a few femtoseconds [1]. They govern thermal effects in solids, e.g., heat capacity, lattice expansion, and phase transitions, and are involved in electron transport phenomena, such as the temperature dependence of the electrical resistance. In combination with free carriers, phonons may lead to static lattice deformations, i.e., polarons, resulting in localization effects of electrons and holes [2,3]. Phonons often dress electronic and magnetic excitations and are responsible for the competition of radiative and nonradiative decay channels or the occurrence of vibronic sidebands in optical spectra. The phonon density of states finally carries unique information on the symmetry and long-range order of crystalline solids [4,5].

The pivotal importance of phonons in solid-state physics entails intense research activities, aiming for an accurate determination of their state-density and electron-coupling constants. Typical experimental schemes are based on neutron, electron, or light scattering and enable phonon detection on macroscopic length scales. Spatially resolved techniques have been pioneered by Ho *et al.*, who established inelastic electron tunneling (IET) spectroscopy with the STM to detect vibrational modes of individual molecules [6]. The vibrational fingerprints are deduced either from energy-transfer processes between tunneling electrons and molecular degrees of freedom [6,7], or vibronic sidebands in STM-luminescence spectra [8,9]. Local measurements of the phonon density of solids are still scarce [10]. One example are IET spectra taken on HOPG, which revealed a complex peak structure coinciding with the symmetry points of phonon bands in graphite [11]. In NaCl thin films, phonon excitations via inelastic electrons were made responsible for the surprisingly large width of gap states induced by Cl vacancies [12]. The broadening was explained with a dressing of electronic resonances by longitudinal optical (LO) phonons in the halide lattice. In ZnO, the LO excitations could be identified directly upon charging or discharging of individual donors with the STM tip [13]. Comparable results were obtained for Cr-doped MgO films, only that the phonon sidebands appeared in the STM-luminescence response in that case and not in the tunneling spectra [14].

In this work, we report a low-temperature STM study on CaO thin films of 7.1 eV band gap grown on a Mo(001) support. We demonstrate that electron transport through the oxide is accompanied by phonon excitations that produce a characteristic signature in the differential conductance (dI/dV) measured across the conduction band (CB) edge. Spatially resolved measurements provide insight into the nature of phonon-assisted electron transport in the presence of lattice defects.

The experiments were performed in an ultrahigh vacuum STM operated at liquid-helium temperature. The CaO films were prepared by Ca deposition onto a clean Mo(001) single crystal in 5×10^{-7} mbar of O_2 [15]. Upon vacuum annealing to 1000 K, the initially amorphous films crystallized and developed a sharp square pattern in LEED, indicative for the (001) termination of rocksalt CaO. STM measurements revealed wide and atomically flat terraces of up to 20 nm diameter, delimited by a network of dislocation lines [Fig. 1(a)]. The films contained traces of Mo that entered the oxide via atom diffusion from the metal substrate during annealing. The Mo ions are responsible for a strong electron-donor character of the material, which controls its reactivity towards electronegative adsorbates, such as oxygen and gold [16].

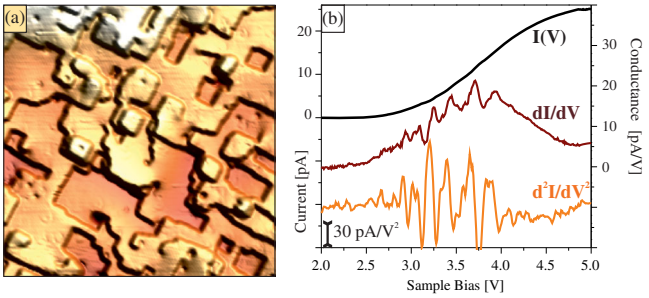

FIG. 1 (color online). (a) STM topographic image of a CaO(001) film of 25 ML thickness ($V_S = 4.5$ V, $I = 25$ pA, 100×100 nm^2). (b) Current, first and second bias derivative of the current, taken across the CB onset on a wide oxide terrace (bias setpoint: 3.5 V).

Because of the insulating character of CaO, low-bias STM images could be exclusively obtained on ultrathin layers, while bias values outside the oxide gap are required to stabilize the tip on thicker films (>10 ML). In the latter regime, electron transport likely proceeds via ballistic or hopping motion through the oxide CB and not via tunneling through the gap region. The operation window for STM is further restricted by a gradual upshift of the CB edge from 2.5 to 4 V when increasing the film thickness to 25 ML [16]. The shift relates to an interface dipole that arises from an electron exchange between Mo donors in the CaO matrix and the metal support. Directly at the interface, the dipole lowers the vacuum energy, hence the position of the oxide bands. With increasing film thickness, it gets progressively screened and the oxide bands shift up again.

The dominance of nontunneling transport through thick CaO films is responsible for a distinct current-voltage characteristic in the STM junction, as measured with the lock-in technique [Fig. 1(b)]. The current starts rising at the CB onset, but quickly saturates at higher bias. Apparently, a conductance channel opens up at the band edge that has, however, finite transport capacity [10,17]. Further current rise is only observed at much higher bias (>5 V), when field emission resonances become available for electron transport through the vacuum region of the tip-sample junction (see Supplemental Material) [18]. More relevant than the total current is the bias-dependent dI/dV response. Also here, a gradual increase of the signal is detected at the CB onset, followed by a maximum and a pronounced decline at higher bias, in good agreement with the saturation behavior of the current. Superimposed on the general shape, we observe characteristic oscillations in the dI/dV intensity [Fig. 1(b)] [7,13]. The fine structure is fully reproduced in subsequent scans and becomes particularly strong in thicker films, for which the in-gap conductance drops to zero. The periodicity of the oscillations is determined from second derivative (d^2I/dV^2) traces, in which the spectral envelop is removed and fitting with a sine becomes possible [Figs. 2(a) and 2(b)]. The analysis reveals a characteristic energy spacing of the maxima that depends on the oxide thickness and the setpoint conditions for spectroscopy. As a general trend, the dI/dV oscillations become more frequent on the bias scale if either the film thickness is reduced or the tip-sample distance is increased, the latter being realized by a higher bias or a lower current setpoint. The mean spacing of dI/dV maxima varies between 70 and 300 mV for films of 5–50 ML thickness, respectively, as shown in Fig. 2(c).

To identify the origin of the dI/dV oscillations, we have first removed possible effects of the STM tip. Because of the insulating character of CaO, the tip electric field is insufficiently screened at the oxide surface and induces a substantial band bending [23,24]. As a result, the applied bias divides into two parts, one dropping in the vacuum gap between tip and sample and the other one inside the oxide film. This voltage division depends on the ratio between tip-sample distance z and oxide thickness d, corrected by the CaO dielectric constant ε_{ox}: $(V_{ox}/V_{vac}) = (d/z)(\varepsilon_{vac}/\varepsilon_{ox})$ [7]. The film thickness was determined via three complementary methods, STM measurements on submonolayer films, analyzing the thickness-dependent LEED pattern, and evaluating the attenuation of Mo $3d$ lines in XPS [15]. The bias-dependent tip-sample distance, on the other hand, was deduced directly from the voltage at the z piezo, adding a constant offset of 5 Å to account for the finite distance at the lowest accessible bias value. After correction, the peak spacing falls into a narrow energy range of $\Delta E = (82 \pm 10)$ meV, and increases only slightly with film thickness [Fig. 2(c)]. The appearance of a unique ΔE value provides evidence that the fine structure in the

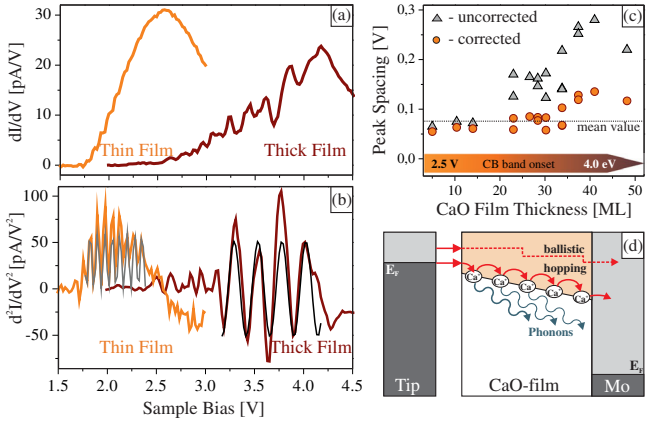

FIG. 2 (color online). (a) Differential conductance spectra and (b) their numerical differentiation taken on 5 and 25 ML thick CaO films. The d^2I/dV^2 traces have been fitted with a sine to determine the bias intervals of the oscillations. (c) Energy associated to the oscillatory behavior of the dI/dV signal, measured for differently thick oxide films and different setpoint conditions. After correction for tip-induced band-bending effects, the energies fall into a narrow range of $\Delta E = (82 \pm 10$ meV). The inset in the bottom visualizes the gradual increase of the CB onset with film thickness. (d) Scheme of ballistic versus hopping transport of electrons through a thick CaO film, including the possible role of phonons.

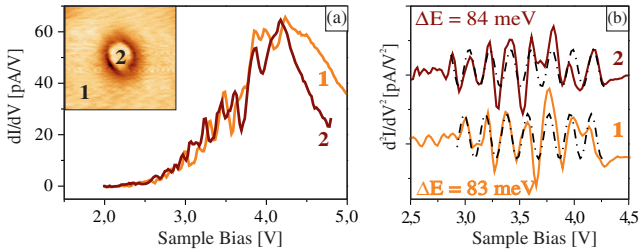

FIG. 3 (color online). (a) Conductance curves measured on top of a subsurface Mo impurity and a defect-free region of a 25 ML thick CaO film. The Mo donor in the inset shows up with a characteristic ring structure, as it temporarily changes the charge state in the tip electric field (5×5 nm^2) [25]. (b) Corresponding second-derivative traces, as used for sine fitting. The derived peak intervals are given in the panel.

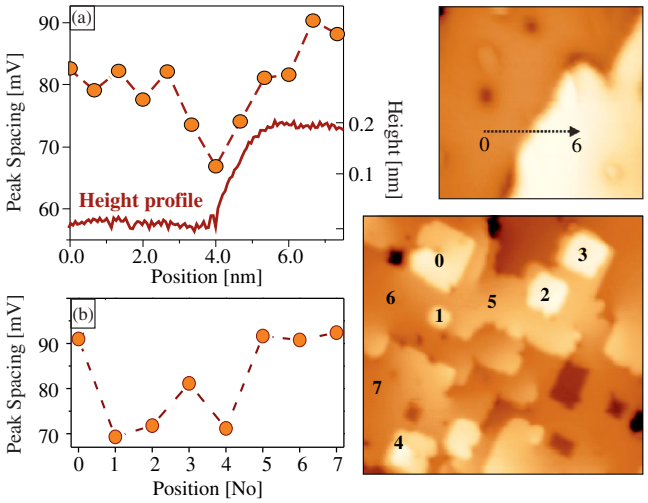

FIG. 4 (color online). (a) Spacing of dI/dV oscillations as determined from a spectral series taken across an oxide dislocation line. The height profile of the defect is depicted as a red line, the corresponding STM topography is shown on the right ($V_S = 4.0$ V, 16×16 nm^2). (b) Characteristic spacing of dI/dV maxima measured either on differently sized ad islands (No. 0–4) or the flat surface (No. 5–7). The right panel shows the associated STM image taken on a 25 ML thick CaO film. ($V_S = 4.0$ V, 40×40 nm^2). All islands are grown around screw dislocations in their center.

dI/dV traces is of physical origin and not related to details of the experiment.

In additional measurements, we have addressed local variations in the dI/dV response across the oxide CB. In Fig. 3, two conductance curves are presented that have been taken on the ideal surface as well as on top of a Mo^{2+} ion in the near-surface region. The latter shows up as a circular feature, as it reversibly changes oxidation state in the tip electric field (Fig. 3, inset) [25]. As before, the conductance behavior is analyzed by evaluating d^2I/dV^2 traces and correcting them for the tip electric field. In both examples, the derived peak spacing is identical within the accuracy of the measurements, suggesting that the Mo impurities do not change the transport properties of the film. A different observation is made on top of CaO edge dislocations, the conductance behavior of which has been accessed by taking a spectral series across the defect line [Fig. 4(a)]. The deduced ΔE value experiences a 10% reduction when approaching the dislocation line, but recovers within 1 nm distance from the defect. A similar behavior is found on nanometer sized CaO islands that typically develop around vertical screw dislocations cutting through the film [Fig. 4(b)]. Also here, the characteristic peak spacing ΔE decreases significantly when the island size becomes smaller than 50 nm^2, but remains constant above this critical value.

The conductance oscillations observed here can be accounted for by two different transport scenarios. In the first case, elastic tunneling into quantized electronic states at the CB onset may produce the regular dI/dV modulations. Such a discrete state density could arise either from electron confinement along the film normal or from in-plane quantization effects. Both possibilities are unlikely. While in the case of vertical confinement, the expected level spacing should decrease with increasing film thickness [26], opposite to the observed trend [Figs. 2(a) and 2(b)], no confining boundaries are obvious within the film plane. Also, a negatively biased tip, as used in our experiment, would not induce a local quantum-well structure, but rather leads to an upward bending of the oxide bands that destroys any confining potentials [27].

In a second scenario, the dI/dV oscillations are interpreted as the spectroscopic fingerprint for inelastic electron transport through the insulating film. As stated before, our CaO films are too thick to enable direct tunneling through the gap region and stable STM operation is only possible for electron injection into the oxide CB. The electrons then move incoherently through the empty band structure, e.g., via hopping motion. If they have sufficient energy to excite one or several quasiparticles in the oxide lattice, maxima may occur in the dI/dV signal as an inelastic transport channel opens up in addition to the elastic one [Fig. 2(d)] [6]. Different quasiparticles have been reported in combination with inelastic electron tunneling in the STM, for instance, polarons, excitons, plasmons, and various magnetic excitations. For a nonmagnetic, wide-gap insulator as CaO, the number of potential excitations with energies below 100 meV reduces essentially to the lattice vibrations, as electronic and optical modes are far too energetic. We thus propose that phonon-assisted electron transport through the CaO film is responsible for the oscillatory dI/dV signal observed here.

In a rough picture, tip electrons are injected into the empty Ca 3s states that constitute the oxide CB. The excess electrons produce temporary lattice distortions, in which adjacent O^{2-} ions are repelled and second nearest Ca^{2+} ions relax towards the Ca^{+} species. When the electrons hop to adjacent Ca sites, the lattice distortion is lifted again and the released energy is emitted in the form of a phonon. This repeated generation and annihilation of lattice distortions produces the characteristic loss features in the differential

conductance. Prior to the first hopping step, only the excess energy of the incoming electron with respect to the CB edge is able to compensate for the phonon-induced losses. Electron injection into the oxide surface is therefore only feasible at bias voltages slightly larger than the actual band onset. With subsequent jumps, the electrons gain energy against the CB bottom that gradually shifts downward in response to the tip-electric field [Fig. 2(d)]. By this means, a driving force is generated for moving the electrons towards the metal-oxide interface, while satisfying the repeated energy request for phonon generation. However, mainly the first energy loss imprints the oscillatory signature onto the dI/dV signal, as here the surface CB provides a well-defined energy reference. This reference gets lost due to the continuous band shift inside the oxide, and the dI/dV maxima smear out after several inelastic jumps of the electrons. We note that thermal excitations at the experimental temperature of 10 K are insufficient to overcome the phonon-induced barrier for electron motion through the CaO film.

Our model also accounts for the observed saturation behavior of the current and the associated drop in the conductance after passing the CB onset [Fig. 1(b)]. Both effects are compatible with an electron transport channel of finite capacity through the CaO film [17]. We assign these limitations to the presence of repulsive Coulomb and strain fields around a Ca ion holding the extra electron. For the lifetime of a phonon excitation, 10^{-12} s, the charged Ca site is blocked for subsequent carriers, which limits its transport capacity to a few nA. Experimental values might be even lower, as several hopping steps are required for an electron to pass the dielectric layer. Inelastic electron transport through the oxide CB accompanied by repeated phonon excitations thus provides a reasonable explanation for the observed conduction characteristic of our STM junction.

In the next step, we focus on details of the electron-phonon interaction that governs charge transport through the CaO lattice. Many ionic crystals exhibit polaron-type conductivity, in which the injected electrons are trapped in a bound state below the CB minimum by inducing a long-lived lattice distortion [2]. Using DFT calculations, we have explored the propensity of CaO to polaron formation. We found that as long as the oxide band gap is properly described, a localized solution for the excess electron is always higher in energy than a delocalized one (Supplemental Material) [18]. Electron localization can be enforced when using hybrid functionals with more than 40% exact Fock exchange; however, this leads to a drastic overestimation of the band gap. A stable polaron is also found on correctly described CaO that contains traces of Mo. While isovalent Mo^{2+} ions are unable to trap electrons, Mo^{3+} and Mo^{4+} impurities produce an attractive Coulomb potential that is susceptible to polaron formation [28]. However, as Mo impurities are mostly of 2+ type in the CaO matrix [25], polaronic effects are not expected to dominate electron transport through the oxide film. This conclusion is in line with the experimental data shown in Fig. 3, which reveal a similar dI/dV behavior for a Mo impurity and the pristine film.

After excluding a dominant polaronic effect, we have searched for phonon modes that match the energy spacing of the dI/dV maxima and may thus be involved in electron hopping through the CaO lattice. In general, LO phonons are known to couple efficiently to moving carriers, as their symmetry renders them sensitive to local modulations in the lattice polarization. In fact, the Γ-point LO phonon of CaO at 71 meV comes closest to the experimental value ($\Delta E = 82$ meV) [29,30]. The remaining discrepancy might be traced back to two factors. First, the LO-phonon energy needs to be renormalized with the empiric Fröhlich coupling constant that describes the effect of a temporary lattice distortion even if no true polaron is formed [31]. The Fröhlich constant has been determined to 1.5 and 2.1 for bulk CaO, using a mean field approximation and Hall measurements, respectively [32,33]. Both values are in line with an increase of the experimental peak spacing with respect to the pure LO mode, although no quantitative agreement is achieved. We mention that a similar trend was recently found for electron tunneling into ZnO(0001) [13]. Second, the deviation of the experimental ΔE value from the bulk LO phonon energy might be ascribed to the limited thickness of the CaO film in our study. Ultrathin films typically experience a phonon softening due to the reduced number of nearest neighbors in the lattice and the dielectric response of the substrate beneath [34,35]. For freestanding CaO films of 1-21 ML thickness, the calculated LO energy indeed increases from 52.2 to 73.3 meV, as discussed in the Supplemental Material [18]. The shift mainly occurs within the first 3 ML, for which no experimental data are available as electron transport is still dominated by direct tunneling. However, the gradual increase of the dI/dV peak spacing with film thickness, even after correcting for the tip electric field, might be a remnant of this phonon softening in ultrathin films [Fig. 2(c)].

Whereas no quantitative agreement between the ΔE value derived from spectroscopy and the LO phonon frequency can be provided at this point, relative trends may be analyzed by cross-correlating the dI/dV oscillations with the CaO morphology obtained from STM images (Fig. 4). On flat and defect-free oxide patches, experimental ΔE values were found to be reasonably constant, while a reproducible 10% decrease in the peak spacing was found around screw and edge dislocations in the surface. We explain this drop with a lower structural order of the CaO lattice around these defects. From x-ray diffraction measurements on isostructural MgO/Mo(001) films [36], we know that the dislocation network is pinned at the metal-oxide interface and penetrates the entire film up to the surface. In addition, the line defects serve as diffusion channels for Mo ions from the support and therefore contain a higher density of impurities. Both effects will modify the phonon characteristic, suggesting that the

reduced spacing of dI/dV maxima might be taken as experimental evidence for a local softening of phonon modes in regions of reduced lattice quality. We want to emphasize that other interpretations cannot be excluded at this point, for instance, that the CaO line defects modify the screening ability of the dielectric film, hence the amount of the band bending in the tip electric field.

In conclusion, STM conductance spectra taken at the CB onset of a thick CaO film exhibit regular dI/dV oscillations that vary with film thickness and experimental setpoint conditions. After correcting the dI/dV traces for the impact of the tip electric field, a unique energy spacing of (82 ± 10) meV is obtained. The underlying excitations are assigned to CaO phonons, being emitted as the electrons move through the oxide lattice. The mode-energy experiences local variations, reflecting the different structural quality of the oxide lattice. Our work demonstrates that new physical phenomena become evident in STM experiments on dielectric films when the dominant electron-transport scheme changes from tunneling to hopping .

This work has been supported by the DFG Excellence Project "UNICAT," the FIRB Project RBAP115AYN, and the COST Action CM1104. Y. C. is grateful for support from the Humboldt Foundation.

*Corresponding author.
nilius@fhi-berlin.mpg.de

[1] G. P. Srivastava, *The Physics of Phonons* (Hilger Pub., Bristol, 1990).
[2] O. F. Schirmer, J. Phys. Condens. Matter **18**, R667 (2006).
[3] A. M. Stoneham, J. Gavartin A. L. Shluger, A. V. Kimmel, D. M. Ramo, H. M. Rønnow, G. Aeppli, and C. Renner, J. Phys. Condens. Matter **19**, 255208 (2007).
[4] R. M. Jaeger, H. Kuhlenbeck, H. J. Freund, M. Wuttig, W. Hoffmann, R. Franchy, and H. Ibach, Surf. Sci. **259**, 235 (1991).
[5] C. Hagendorf, S. Sachert, B. Bochmann, K. Kostov, and W. Widdra, Phys. Rev. B **77**, 075406 (2008).
[6] B. C. Stipe, M. A. Rezaei, and W. Ho, Science **279**, 1907 (1998); W. Ho, J. Chem. Phys. **117**, 11033 (2002).
[7] S. W. Wu, G. V. Nazin, X. Chen, X. H. Qiu, and W. Ho, Phys. Rev. Lett. **93**, 236802 (2004).
[8] X. H. Qiu, G. V. Nazin, and W. Ho, Science **299**, 542 (2003).
[9] E. Ćavar, M.-C. Blüm, M. Pivetta, F. Patthey, M. Chergui, and W.-D. Schneider, Phys. Rev. Lett. **95**, 196102 (2005).
[10] M. Berthe, R. Stiufiuc, B. Grandidier, D. Deresmes, C. Delerue, and D. Stiévenard, Science **319**, 436 (2008).
[11] L. Vitali, M. A. Schneider, K. Kern, L. Wirtz, and A. Rubio, Phys. Rev. B **69**, 121414 (2004).
[12] J. Repp, G. Meyer, S. Paavilainen, F. E. Olsson, and M. Persson, Phys. Rev. Lett. **95**, 225503 (2005).
[13] H. Zheng, J. Kröger, and R. Berndt, Phys. Rev. Lett. **108**, 076801 (2012).
[14] F. Stavale, N. Nilius, and H.-J. Freund, New J. Phys. **14**, 033006 (2012).
[15] X. Shao, P. Myrach, N. Nilius, and H.-J. Freund, J. Phys. Chem. C **115**, 8784 (2011).
[16] Y. Cui, X. Shao, M. Baldofski, J. Sauer, N. Nilius, and H.-J. Freund, Angew. Chem., Int. Ed. **52**, 11385 (2013); X. Shao, S. Prada, L. Giordano, G. Pacchioni, N. Nilius, and H. J. Freund, Angew. Chem., Int. Ed. **50**, 11525 (2011).
[17] M. Berthe *et al.*, Phys. Rev. Lett. **97**, 206801 (2006).
[18] See Supplemental Material at http://link.aps.org/supplemental/10.1103/PhysRevLett.114.016804, which includes Refs. (19–22).
[19] R. Dovesi, R. Orlando, B. Civalleri, C. Roetti, V. R. Saunders, and C. M. Zicovich-Wilson, Z. Kristallogr. **220**, 571 (2005).
[20] L. Valenzano, F. J. Torres, K. Doll, F. Pascale, C. M. Zicovich-Wilson, and R. Dovesi, Z. Phys. Chem. (Frankfort/Main) **220**, 893 (2006); E. Ruiz, M. Llunell, and P. Alemany, J. Solid State Chem. **176**, 400 (2003).
[21] A. D. Becke, J. Chem. Phys. **98**, 5648 (1993); C. Lee, W. Yang, and R. G. Parr, Phys. Rev. B **37**, 785 (1988).
[22] M. Ferrero, M. Rerat, R. Orlando, and R. Dovesi, J. Comput. Chem. **29**, 1450 (2008); M. Ferrero, M. Rerat, B. Kirtman, and R. J. Dovesi, J. Chem. Phys. **129**, 244110 (2008).
[23] R. M. Feenstra, Phys. Rev. B **50**, 4561 (1994).
[24] G. J. de Raad, D. M. Bruls, P. M. Koenraad, and J. H. Wolter, Phys. Rev. B **66**, 195306 (2002).
[25] Y. Cui, N. Nilius, H.-J. Freund, S. Prada, L. Giordano, and G. Pacchioni, Phys. Rev. B **88**, 205421 (2013).
[26] D. A. Evans, M. Alonso, R. Cimino, and K. Horn, Phys. Rev. Lett. **70**, 3483 (1993).
[27] T. Maltezopoulos, A. Bolz, C. Meyer, C. Heyn, W. Hansen, M. Morgenstern, and R. Wiesendanger, Phys. Rev. Lett. **91**, 196804 (2003).
[28] S. Prada, L. Giordano, and G. Pacchioni, J. Phys. Chem. C **117**, 9943 (2013).
[29] J. T. Gourley and W. A. Runciman, J. Phys. C **6**, 583 (1973).
[30] D. H. Saunderson and G. E. Peckham, J. Phys. C **4**, 2009 (1971).
[31] H. Fröhlich, H. Pelzer, and S. Zienau, Philos. Mag. **41**, 221 (1950).
[32] K. Tanimura, Phys. Rev. B **63**, 184303 (2001).
[33] Landolt-Börnstein-Condensed Matter, *II-VI and I-VII Compounds; Semimagnetic Compounds* (Springer, New York, 1999), Vol. 41B, p. 1.
[34] A. Gonchar, T. Risse, H.-J. Freund, L. Giordano, C. Di Valentin, and G. Pacchioni, Angew. Chem., Int. Ed. **50**, 2635 (2011).
[35] L. Savio, E. Celasco, L. Vattuone, M. Rocca, and P. Senet, Phys. Rev. B **67**, 075420 (2003).
[36] S. Benedetti, P. Torelli, S. Valeri, H. M. Benia, N. Nilius, and G. Renaud, Phys. Rev. B **78**, 195411 (2008).